Notice

Manuscript details

Title: Does a damaged-fault zone mitigate the near-field impact of supershear earthquakes?—Application to the 2018 Mw 7.5 Palu earthquake

Authors: Elif Oral, Huihui Weng and Jean-Paul Ampuero

Contact: elif.oral@geoazur.unice.fr

Does a damaged-fault zone mitigate the near-field impact of supershear earthquakes?—Application to the 2018 M_w 7.5 Palu earthquake

Elif Oral[1], Huihui Weng[1], and Jean Paul Ampuero[1,2]

[1]Université Côte d'Azur, IRD, CNRS, Observatoire de la Côte d'Azur, Géoazur, France
[2]California Institute of Technology, Seismological Laboratory, Pasadena, CA, USA

Key Points:

- The unexpectedly low rupture speed of the 2018 Palu supershear earthquake can be explained by a fault damage zone.
- The reduction of rupture speed by a fault damage zone mitigates the near-field ground motion and landslide hazard.
- Fault zone waves amplify ground motions, but not enough to compensate for the mitigation effect of rupture speed.

Corresponding author: Elif Oral, `elif.oral@geoazur.unice.fr`

Abstract

The impact of earthquakes can be severely aggravated by cascading secondary hazards. The 2018 M_w 7.5 Palu, Indonesia earthquake led to devastating tsunamis and landslides, while triggered submarine landslides possibly contributed substantially to generate the tsunami. The rupture was supershear over most of its length, but its speed was unexpectedly low, between the S-wave velocity V_S and Eshelby's speed $\sqrt{2}V_S$, an unstable speed range in conventional theory. Here, we investigate whether dynamic rupture models including a low-velocity fault zone (LVFZ) can reproduce such steady, slow supershear rupture. We then examine numerically how this peculiar feature of the Palu earthquake could have affected the near-field ground motion and thus the secondary hazards. Our findings suggest that the presence of a LVFZ can explain the slowness of the rupture and may have mitigated the near-field ground motion and induced landslides in Palu.

Plain Language Summary

Earthquakes are produced by slippage quickly unzipping along faults, causing Earth's vibrations that we feel as ground shaking. The shaking can become more catastrophic by triggering other phenomena, like landslides and tsunamis, as did the 2018 Palu (Indonesia) earthquake of magnitude 7.5. Generally, the faster the earthquake rupture, the stronger the shaking. The Palu earthquake is among a class of very fast but rare earthquakes whose speed exceeds that of shearing waves in rocks. Theoretically these so-called "supershear earthquakes" can propagate steadily only if faster than a speed known as Eshelby's speed; Surprisingly, the Palu earthquake is slower than this limit. How can we explain this slow, steady supershear rupture in Palu? How does it affect the potential of triggering landslides, including submarine landslides that likely contributed to the tsunami. We address these questions through computer simulations, particularly focusing on the possible effect of a "fault damage zone"—softened rocks surrounding faults because of accumulated rock fracturing throughout the past fault activity. We found that, if a damage zone exists around the Palu fault, it can explain the slow supershear and may have had the beneficial effect of reducing the shaking, and thus its induced landslide and tsunami hazards in Palu.

1 Introduction

The 2018 M_w 7.5 earthquake in Palu, Sulawesi, Indonesia, ruptured at a supershear speed. The rupture initiated on an unmapped fault located within the inland Sulawesi neck and propagated 150 km southward on the strike-slip Palu-Koro fault. Studies using teleseismic back-projection revealed that the rupture reached rapidly a steady velocity of about V_{rup}=4.1 km/s, exceeding the local S-wave velocity V_S=3.4-3.8 km/s (Bao et al., 2019).

The rupture speed of the Palu earthquake was unexpectedly low as a supershear earthquake, and here we aim at understanding whether the presence of a damaged-fault zone can be the reason behind it. On the basis of theoretical and experimental studies, a stable rupture propagation at supershear speed is only expected at velocities higher than Eshelby's speed $V_E = \sqrt{2}V_S$ (e.g., Andrews, 1976; Dunham, 2007). Yet, the inferred rupture speed of the Palu event lies in the unstable supershear regime $V_S < V_{rup} < V_E$. One proposed explanation of such a rupture speed is the presence of a low-velocity fault zone (LVFZ). Supershear ruptures in a LVFZ approach the P-wave speed of the LVFZ (Huang et al., 2016). Indeed, Bao et al. (2019) interpreted the observed rupture speed by the possible presence of a LVFZ with 30% velocity reduction. However, previous studies modeling supershear rupture in a LVFZ were based on 2D models that ignored the finiteness of the seismogenic depth, while the Palu earthquake rupture has a high length-to-width ratio (150 km length vs. a typical seismogenic depth of 15-20 km for strike-slip earthquakes). Recent theory and simulations show that the seismogenic width controls the evolution of rupture speed in elongated faults (Weng & Ampuero, 2019). Thus, the first question we address, in section 2, is: can the presence of a LVFZ lead to a slow steady-state supershear rupture (running at the damaged-P-wave speed) in a long rupture with finite seismogenic width?

The earthquake also triggered devastating landslides; the rupture properties must have been determinant on the distribution and density of co-seismic landslides. The impact of the earthquake was aggravated by landslides triggered in the proximity of the fault, including submarine landslides in the Palu Bay that likely contributed to the generation of a devastating tsunami (Carvajal et al., 2019). Major co-seismic landslides were reported in four different areas, within 10 km of distance from the fault, on gently-sloping alluvial valley floor (Bradley et al., 2019). Past studies have relied on the empirical evaluation of earthquake-induced landslide hazard by using seismic factors such as earthquake magnitude and epicentral distance (e.g., Keefer, 1984; Papadopoulos & Plessa, 2000; Meunier et al., 2007). Yet, recent research points to the necessity of considering the combined effect of geo-environmental factors and rupture complexities to improve the hazard prediction. For example, landslides triggered by the 2008 Wenchuan earthquake were found to be unexpectedly high for a M_w 7.9 event (Xu et al., 2016). Conversely, 1999 M_w 7.2 Düzce and the 2002 M_w 7.9 Denali earthquakes have induced landslides lower than expected for M7+ earthquakes (Görüm et al., 2011). Indeed, despite the similarities of magnitude, topology, climate and rock type, the difference between the 2015 M_w 7.8 Gorkha and the 2008 Wenchuan earthquake-triggered landslide densities is mainly associated with the rupture complexities (Xu et al., 2016; Roback et al., 2018). For that reason, we also investigate the effect of rupture properties of the Palu earthquake on ground motion and consequent landslide triggering in the near field.

We scope to clarify whether the ground motion and the consequent landslide-triggering impact during the Palu earthquake were mitigated by the lower rupture speed or aggravated by wave amplification due to a damage zone. Among the source properties, rupture speed significantly affects ground motion: a supershear rupture can generate stronger ground motion than a subshear rupture, except if the rupture propagates at sub-Eshelby speed (Aagaard & Heaton, 2004; Dunham & Archuleta, 2005; Bizzarri & Spudich, 2008). On the other hand, waves trapped by a LVFZ can amplify ground motion (Spudich & Olsen, 2001; Ben-Zion et al., 2003; Peng et al., 2003; Huang et al., 2014; Kurzon et al., 2014). The Palu earthquake is a sub-Eshelby supershear rupture (relative to the host-rock wave speed) and may have occurred within a LVFZ: rupture speed and fault zone structure may have had competing effects on ground motion. Therefore, the second question we address, in section 3, is: in the presence of a LVFZ, can a supershear rupture running at the damaged-P-wave speed aggravate near-field ground motion?

2 Early and sustained supershear at damaged-P-wave speed

2.1 2.5D dynamic rupture modeling

We model a dynamic rupture on a vertical strike-slip fault with finite seismogenic width W. For the sake of computational efficiency, we adopt a reduced-dimensionality (2.5D) model, which has been shown to be a successful approximation of 3D rupture mod-

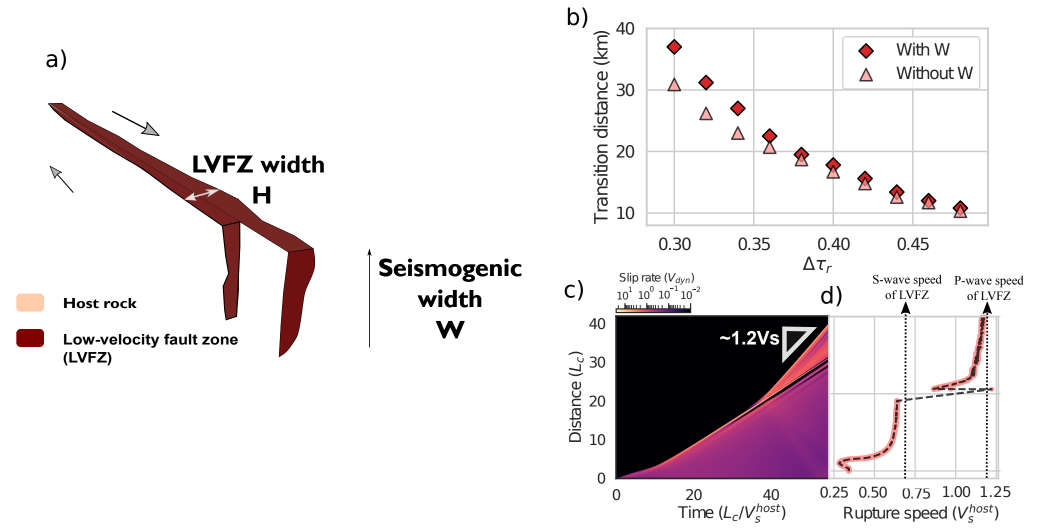

Figure 1. (a) Conceptual model of a low-velocity fault zone. (b) Supershear transition distance as a function of stress drop (normalized by strength drop) in dynamic rupture models with and without finite seismogenic zone. (c) Spatio-temporal distribution of slip rate and (d) rupture speed vs distance along the fault strike for the simulation where $\Delta\tau_r = 0.37$.

els on elongated faults (Weng & Ampuero, 2019). The fault bisects a LVFZ with uniform properties, embedded in an unbounded, homogeneous host rock medium (Figure 1a). The LVFZ is defined by its width H and its reduction of P- and S-wave velocities relative to the host rock, $\Delta V/V$. We set $\Delta V/V = 30\%$, as hypothesized by Bao et al. (2019). Such a value of velocity reduction is not unusual in mature fault zones (Huang & Ampuero, 2011). We set a Poisson's ratio of 0.25 everywhere.

We artificially initiate the rupture by prescribing a smooth time-weakening front that expands at a prescribed speed, $0.25V_s$, as in Andrews (1985). The rupture starts to propagate spontaneously when the time-weakening front exceeds a critical nucleation length. Outside the time-weakening zone, the fault is controlled by the linear slip-weakening friction law (Ida, 1972; Palmer & Rice, 1973), with static and dynamic friction coefficients $\mu_s = 0.6$ and $\mu_d = 0.1$, respectively, and critical slip distance D_c.

We normalize all spatial parameters by the characteristic frictional length $L_c = GD_c/\sigma(\mu_s - \mu_d)$, where G is the shear modulus and σ is the fault normal stress. This length is proportional to the process-zone size that must be well resolved by the numerical grid (Day et al., 2005). Due to computational constraints, we assume $L_c = 400$ m.

Huang et al. (2016) found a correlation between supershear-transition distance, normalized LVFZ width H/L_c and initial background stress. We quantify the initial background stress by the ratio $\Delta\tau_r$ of stress drop (difference between initial shear stress and dynamic shear strength $\sigma\mu_d$) to strength drop $\sigma(\mu_s - \mu_d)$. For a given $\Delta\tau_r$, the supershear-transition distance increases as a function of H/L_c. Here, we set $H = 2L_c$ to mimic the early superhear transition of the Palu earthquake for a considerably wide range of initial stress conditions. LVFZ widths most often range between 100 and 400 m, with some exceptions exceeding 1 km (Huang & Ampuero, 2011). In our model, the LVFZ width equals 800 m. We set the seismogenic width as $W = 30L_c$, which corresponds to 12 km.

The simulations are done with the spectral element code SEM2DPACK (Ampuero, 2002, 2012). We set the element size sufficiently small to resolve the process-zone size: $0.1L_c$ and $0.5L_c$ with 9 Gauss-Lobatto-Legendre (GLL) nodes per element edge in the LVFZ and host-rock media, respectively. Numerical oscillations are mitigated by artificial damping around the fault. The model domain and the duration of the simulation are chosen such that the rupture does not reach the fault end, and spurious numerical reflections at the model boundaries do not reach the rupture. Perfectly Matched Layers are imposed at all model boundaries.

2.2 Results

Our analyses show that, even when accounting for the finite seismogenic width, the supershear transition can occur early if the background stress is sufficiently high. We performed simulations at different background stress ratios ranging from 0.2 to 0.48. Figure 1 (b) shows the supershear-transition distance for each case, compared to the results without W-effect (2D simulations equivalent to $W = \infty$). The transition occurs at shorter distances for a higher initial stress. This trend is qualitatively similar to that in the infinite-W case; the effect of the seismogenic depth slightly delays the supershear transition, by less than 20%. The calculated transition distance ranges roughly from 4 to 15 km if $\Delta\tau_r$ ranges from 0.3 to 0.5. Considering the uncertainties of relative location in the back-projection imaging of the Palu earthquake by Bao et al. (2019), these models are consistent with the observed early supershear-transition distance.

The observed rupture speed of the Palu event is not surprisingly low for a damaged fault; the presence of a LVFZ can induce a steady-state supershear rupture at the damaged-P-wave speed, even on an elongated fault. We further present the rupture properties in one of the cases where the supershear transition distance is consistent with the observation, namely the case $\Delta\tau_r = 0.37$. The distribution of slip rate as a function of distance along strike and time is shown in Figure 1 (c). The rupture is initially sub-shear and transitions to supershear at a distance of 20 L_c (corresponding to 8 km). The rupture speed stabilizes at $\sim 1.2V_s$ (Figure 1d), which is the P-wave speed of the LVFZ medium. Given the observed rupture speed, 4.1 km/s, for an approximate S-wave speed of host rock of 3.5 km/s for the Palu event, the results of our dynamic rupture modeling support the possibility that the LVFZ presence promotes a persistent slow supershear rupture at damaged-P-wave speed.

Slow supershear events as the Palu earthquake should not be surprising for major faults with a pronounced damage zone. Although we focused above on a single set of parameters that represents well the short supershear-transition distance and slow rupture features of the Palu event, given that we found the W-effect is not dramatic, the effect of different values of fault zone width and velocity reduction can be anticipated based on the findings of comprehensive sensitivity analyses in 2D by Huang and Ampuero (2011); Huang et al. (2014, 2016). According to these studies, the presence of a LVFZ leads to a lower critical stress value for supershear transition than in homogeneous media, owing to dynamic stress perturbations induced by fault zone waves. Moreover, the rupture speed depends on initial stress and LVFZ properties. If the LVFZ is too narrow (e.g., $H <\sim L_c$ if $\Delta V/V = 30\%$) the wavelength of head waves inside the LVFZ is too short to induce a permanent supershear transition at any initial stress level. If the LVFZ is too wide ($H > 6L_c$ if $\Delta V/V = 30\%$) very long distances ($> 100L_c$) or high initial stress values ($\Delta\tau_r > 0.45$) are required to promote supershear speed. Thus, for the case with 30% velocity reduction, the range of LVFZ widths that likely promotes slow supershear rupture is $1 < H/L_c < 6$. This condition implies LVFZ widths ranging from 400 m to 2.4 km for our particular choice of L_c value. Such range involves values near and above the upper end of real LVFZ widths. A smaller L_c value allows for slow supershear rupture well within the usual range of natural LVFZ widths. Therefore, rupture propagation at the speed of the Palu earthquake can be expected under a considerably wide range of conditions, supporting the slow supershear hypothesis of Huang et al. (2016)

for past earthquakes such as the 1906 San Francisco and the 1999 M_w 7.1 Düzce earthquakes (Ben-Zion et al., 2003; Song et al., 2008). Better constraining LVFZ properties and L_c could help to test further this hypothesis.

3 Changes in near-field ground motion during a slow supershear rupture

3.1 3D wave propagation modeling

To investigate the near-field ground motions during a persistent supershear rupture, we simulated steady-state ruptures in 3D, with prescribed constant stress drop and constant rupture speed. Following the procedure of Andrews (1985) and Dunham and Bhat (2008), we force the friction coefficient to weaken linearly as a function of time inside a process zone, which propagates at prescribed speed. At the tail of the process zone, the friction coefficient equals μ_d. To avoid stress singularities at the rupture tip, the peak fault strength and process zone size are not prescribed but vary spontaneously.

We created three different models: Model A is a fast supershear model without LVFZ; Model B is a slow supershear model with a LVFZ; and Model C is a slow supershear model without LVFZ. We set V_S= 3.5 km/s for all models, such that V_P=6.06 km/s, V_E=4.95 km/s, and Poisson's ratio is 0.25. We set the rupture speed in Model A as 5.95 km/s, close to the P-wave speed; and in Models B and C as 4.17 km/s, a sub-Eshelby speed. The element sizes are 0.4 and 1.2 km in the LVFZ and host-rock media, respectively. 5 GLL points are used per spectral element edge. The grid allows for a resolution up to 2 Hz; we apply a Butterworth low-pass filter with 2 Hz corner frequency to all simulated signals before analysis. The model length, width and depth are 360 km, 180 km and 36 km, respectively. We set the seismogenic width to 12 km. Spurious numerical reflections from model boundaries are mitigated by absorbing boundary layers. We let the rupture propagate a distance of 72 km (that is, 6 W). The simulations are conducted with the SPECFEM3D software (Kaneko et al., 2008; Tromp et al., 2008; Galvez et al., 2014). We verified that the final slip is similar in the three models (differences are of about 10 %).

We evaluated the induced-landslide potential, in relative terms, by comparing seismic intensity parameters. Many studies of co-seismic landslide susceptibility have used seismic intensity parameters such as peak ground velocity (PGV), peak ground acceleration (PGA) and Arias intensity (I_a). Several quantitative analyses on past co-seismic

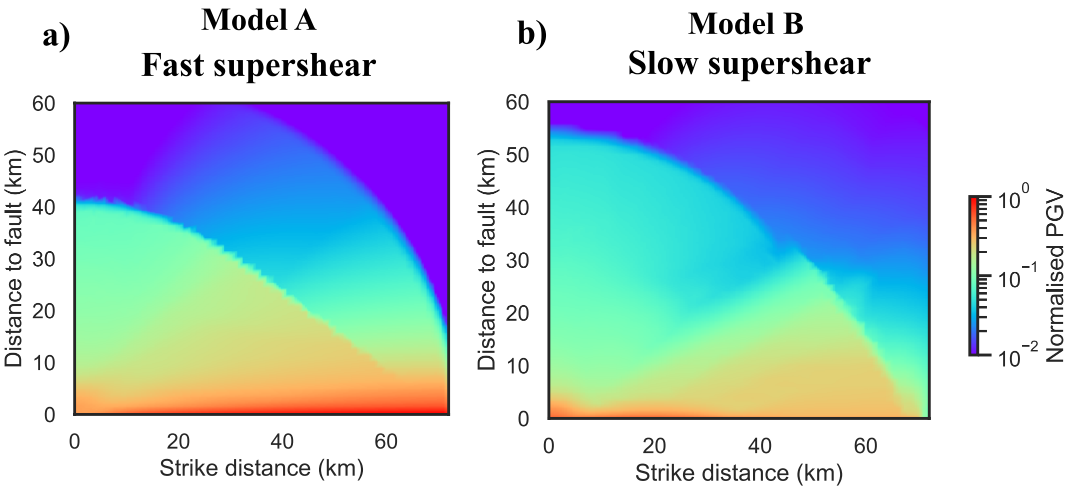

Figure 2. Maximum peak-to-peak amplitude of ground velocities for (a) fast supershear and (b) slow supershear models. All values are normalized by the maximum value of Model A.

landslides also point to the correlation between these parameters and observed distribution patterns of landslides (e.g., Refice & Capolongo, 2002; Meunier et al., 2007). Although the combined use of these parameters has been proposed to improve the prediction of landslide displacement (Saygılı & Rathje, 2008), a recent comparative study suggests that all parameters produce similar results (Dreyfus et al., 2013). Therefore, in this study, we discuss the landslide-triggering impact of ground motion by using PGV. Given the limitations of our simulations to low frequency (< 2 Hz), we provide PGA and I_a results only for reference in supplementary material.

3.2 Mitigation of near-field landslide hazard by sub-Eshelby rupture speed

Peak ground motion is notably attenuated due to the reduction of rupture speed. As expected, P waves attenuate with distance in both models, and large S-wave amplitudes persist to long distances within Mach cones (Figure 2). The overall spatial extension of the highest PGV values is wider in Model A than in Model B given the wide expansion of the Mach cone in Model A due to its high rupture speed.

The reduction in ground-motion amplitude is related to the significant attenuation of waves in the whole frequency band due to the slow supershear speed. We compare the acceleration spectra between Models A and B at a strike distance of 40 km (Figure S1.1).

When the rupture front reaches a distance of 72 km, the Mach cone of Model A has propagated to 22 km off the fault at 40 km along strike. Within this distance, the ground motion in Model B is weaker than in Model A at all frequencies (except for the partial amplification of low-frequency motion of Model B close to the fault in the fault-normal direction). This damping effect affects all components of ground motion at the same distance (Figure S1.2).

To mimic the landslide-triggering impact of our models on reported landslide locations of the Palu earthquake, we evaluate the ground motion at a fixed along-strike distance. Both submarine and inland landslides of the Palu earthquake are reported at locations that are considerably far from the fault end, and where the rupture presumably propagated at a steady state. In addition, these sites are located at comparable distances in units of W, such that we interpret the landslide hazard of these sites by analyzing the ground motion at different off-fault distances but at a fixed along-strike distance.

The analyses on peak-ground velocities point to the reduction of landslide-triggering potential in the slow supershear model. We compare the dependence of PGV on off-fault distance at a strike distance of 40 km—we verified that the rupture reached steady state there—between Models A and B (Figure 3a). The largest values occur in the vicinity of the fault in both models, and the difference of PGV between the models vanishes with increasing distance to the fault. Within the distance of Mach-front propagation ($<$ 22 km), the PGV values of the fast supershear model are higher than those of the slow supershear model.

Our results support the findings of past studies: a smaller rupture speed (here caused by the presence of a LVFZ) results in a significant reduction of the amplitudes of near-field ground motion and consequent landslide-triggering impact, and this influence of rupture speed on ground motion is valid at various distances from the fault (within 30 km here).

3.3 Enhanced high-frequency ground motion and landslide hazard caused by damage

High-frequency waves are amplified due to the damaged-fault zone over a wide range of off-fault distances. To isolate the effect of the presence of a LVFZ, we compare two

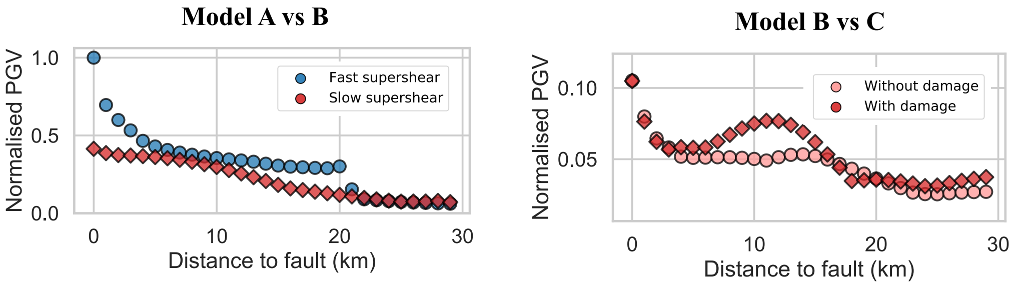

Figure 3. Comparison of peak ground velocities vs distance from the fault between fast (Model A) and slow (Model B) supershear models (a), and between slow supershear models with damage (Model B) and without damage (Model C) (b). All values are normalized by the maximum value of the Model A.

slow supershear models with and without LVFZ (Models B and C, respectively). Our analysis of acceleration spectra suggests that the presence of a LVFZ results in slight amplification of the ground motion, in particular at frequencies above 0.5 Hz (Figure S1.4). This is expected, since the resonance frequency of waves normally reflected at the LVFZ-host rock interface is 0.39 Hz.

The high-frequency amplification due to the damaged-fault zone leads to the increase of landslide-triggering impact based on our analyses. We compare the PGV values of the two models in Figure 3 (b). In both, PGV decays with off-fault distance; but in the presence of a LVFZ (model B), the PGV values are amplified because of enhanced high-frequency radiation. To well constrain the effect of the LVFZ, we made the comparison in the frequency band of 0.5-2 Hz; PGV amplification due to the LVFZ at a strike distance of 40 km is pronounced particularly between approximately 6 and 16 km.

The reflections due to the velocity contrast between the LVFZ and host rock can result in an amplified high-frequency motion that could also increase the landslide-triggering impact at farther distances to the fault. Considering the extent of the sites where landslides are reported, our results indicate that the landslide triggering potential of the Palu earthquake may have been aggravated by the presence of a damaged-fault zone (comparison of Model B and C). Yet, in the previous subsection, we found a dampening effect of the LVFZ on landslide triggering potential, via its effect on rupture velocity (comparison of Model A and B). Out of these two competing effects of the LVFZ, the former one (amplification) is relatively slight.

4 Conclusions and Discussion

Our 2.5D dynamic rupture models of the Palu earthquake suggest that, also for elongated-fault ruptures that saturate the seismogenic thickness, the presence of a damaged-fault zone can promote an early and persistent supershear rupture at a speed that is unexpectedly slow for intact rock, namely the P-wave speed of the damaged rock.

The near-field ground motion produced by a supershear rupture is much weaker if it runs at the damaged-P-wave speed and if this speed is lower than the Eshelby's speed of the host rock. The presence of a damaged-fault zone also amplifies high-frequency ground motion (> 0.5 Hz) up to long distances from the fault (30 km). Yet, the latter effect is weaker, thus overall the presence of a LVFZ mitigates the near-field ground motion and its landslide triggering potential.

Our findings support the strong influence of the rupture dynamics and fault zone structure on near-field ground motion and earthquake-induced landslides. The results of our simplified modeling can serve as a reference for more realistic studies where topography, heterogeneous material properties, and liquefaction potential are accounted for on a broader frequency band.

Our results can be helpful for further understanding the role of low-velocity fault zones on past and future earthquakes (e.g., Perrin et al., 2016). For example, the presence of a damaged-fault zone was speculated as an explanation of the difference of rupture speed between the northern and southern sides of the fault during the 1999 M_w 7.4 İzmit earthquake (Bouchon et al., 2001). Mai (2019) draws attention to the striking similarities between the İzmit and Palu cases for further earthquake mitigation programs—the rupture of İzmit earthquake also propagated for 150 km on a strike-slip fault; and co-seismic tsunamis were triggered and locally amplified presumably because of tectonic subsidence and submarine landslides within the narrow İzmit Bay (Yalçıner et al., 2000).

Acknowledgments

This work was supported by the French National Research Agency (ANR) through project FAULTS_R_GEMS (grant ANR-17-CE31-0008) and Investments-in-the-Future project

UCAJEDI (grant ANR-15-IDEX-01). We acknowledge Luis A. Dalguer for helpful comments that improved the content of this manuscript. All data to reproduce this work is available online: 2D and 3D wave propagation modeling tools can be found at `https://github.com/jpampuero/sem2dpack` and `https://github.com/geodynamics/specfem3d` addresses.

References

Aagaard, B. T., & Heaton, T. H. (2004). Near-source ground motions from simulations of sustained intersonic and supersonic fault ruptures. *Bulletin of the Seismological Society of America*, *94*(6), 2064–2078.

Ampuero, J.-P. (2002). Etude physique et numérique de la nucléation des séismes. *PhD Thesis, University of Paris VII, France*.

Ampuero, J.-P. (2012). A spectral element method tool for 2d wave propagation and earthquake source dynamics users guide.

Andrews, D. (1976). Rupture velocity of plane strain shear cracks. *Journal of Geophysical Research*, *81*(32), 5679–5687.

Andrews, D. (1985). Dynamic plane-strain shear rupture with a slip-weakening friction law calculated by a boundary integral method. *Bulletin of the Seismological Society of America*, *75*(1), 1–21.

Bao, H., Ampuero, J.-P., Meng, L., Fielding, E. J., Liang, C., Milliner, C. W., … Huang, H. (2019). Early and persistent supershear rupture of the 2018 magnitude 7.5 palu earthquake. *Nature Geoscience*, *12*(3), 200–205.

Ben-Zion, Y., Peng, Z., Okaya, D., Seeber, L., Armbruster, J. G., Ozer, N., … Aktar, M. (2003). A shallow fault-zone structure illuminated by trapped waves in the karadere–duzce branch of the north anatolian fault, western turkey. *Geophysical Journal International*, *152*(3), 699–717.

Bizzarri, A., & Spudich, P. (2008). Effects of supershear rupture speed on the high-frequency content of s waves investigated using spontaneous dynamic rupture models and isochrone theory. *Journal of Geophysical Research: Solid Earth*, *113*(B5).

Bouchon, M., Bouin, M.-P., Karabulut, H., Toksöz, M. N., Dietrich, M., & Rosakis, A. J. (2001). How fast is rupture during an earthquake? new insights from the 1999 turkey earthquakes. *Geophysical Research Letters*, *28*(14), 2723–2726.

Bradley, K., Mallick, R., Alfian, D., Andikagumi, H., Benazir, B., Brocard, G., … others (2019). Wet rice cultivation was the primary cause of the earthquake-triggered palu landslides.

Carvajal, M., Araya-Cornejo, C., Sepúlveda, I., Melnick, D., & Haase, J. S. (2019). Nearly instantaneous tsunamis following the mw 7.5 2018 palu earthquake. *Geophysical Research Letters*, *46*(10), 5117–5126.

Day, S. M., Dalguer, L. A., Lapusta, N., & Liu, Y. (2005). Comparison of finite difference and boundary integral solutions to three-dimensional spontaneous rupture. *Journal of Geophysical Research: Solid Earth*, *110*(B12).

Dreyfus, D., Rathje, E. M., & Jibson, R. W. (2013). The influence of different simplified sliding-block models and input parameters on regional predictions of seismic landslides triggered by the northridge earthquake. *Engineering geology*, *163*, 41–54.

Dunham, E. M. (2007). Conditions governing the occurrence of supershear ruptures under slip-weakening friction. *Journal of Geophysical Research: Solid Earth*, *112*(B7).

Dunham, E. M., & Archuleta, R. J. (2005). Near-source ground motion from steady state dynamic rupture pulses. *Geophysical Research Letters*, *32*(3).

Dunham, E. M., & Bhat, H. S. (2008). Attenuation of radiated ground motion and stresses from three-dimensional supershear ruptures. *Journal of Geophysical Research: Solid Earth*, *113*(B8).

Galvez, P., Ampuero, J.-P., Dalguer, L. A., Somala, S. N., & Nissen-Meyer, T. (2014). Dynamic earthquake rupture modelled with an unstructured 3-d spectral element method applied to the 2011 m 9 tohoku earthquake. *Geophysical Journal International*, *198*(2), 1222–1240.

Görüm, T., Fan, X., van Westen, C. J., Huang, R. Q., Xu, Q., Tang, C., & Wang, G. (2011). Distribution pattern of earthquake-induced landslides triggered by the 12 may 2008 wenchuan earthquake. *Geomorphology*, *133*(3-4), 152–167.

Huang, Y., & Ampuero, J.-P. (2011). Pulse-like ruptures induced by low-velocity fault zones. *Journal of Geophysical Research: Solid Earth*, *116*(B12).

Huang, Y., Ampuero, J.-P., & Helmberger, D. V. (2014). Earthquake ruptures modulated by waves in damaged fault zones. *Journal of Geophysical Research: Solid Earth*, *119*(4), 3133–3154.

Huang, Y., Ampuero, J.-P., & Helmberger, D. V. (2016). The potential for supershear earthquakes in damaged fault zones–theory and observations. *Earth and Planetary Science Letters*, *433*, 109–115.

Ida, Y. (1972). Cohesive force across the tip of a longitudinal-shear crack and griffith's specific surface energy. *Journal of Geophysical Research*, *77*(20), 3796–3805.

Kaneko, Y., Lapusta, N., & Ampuero, J.-P. (2008). Spectral element modeling of spontaneous earthquake rupture on rate and state faults: Effect of velocity-strengthening friction at shallow depths. *Journal of Geophysical Research: Solid Earth*, *113*(B9).

Keefer, D. K. (1984). Landslides caused by earthquakes. *Geological Society of America Bulletin*, *95*(4), 406–421.

Kurzon, I., Vernon, F. L., Ben-Zion, Y., & Atkinson, G. (2014). Ground motion prediction equations in the san jacinto fault zone: Significant effects of rupture directivity and fault zone amplification. *Pure and Applied Geophysics*, *171*(11), 3045–3081.

Mai, P. M. (2019). Supershear tsunami disaster. *Nature Geoscience*, *12*(3), 150.

Meunier, P., Hovius, N., & Haines, A. J. (2007). Regional patterns of earthquake-triggered landslides and their relation to ground motion. *Geophysical Research Letters*, *34*(20).

Palmer, A. C., & Rice, J. R. (1973). The growth of slip surfaces in the progressive failure of over-consolidated clay. *Proceedings of the Royal Society of London. A. Mathematical and Physical Sciences*, *332*(1591), 527–548.

Papadopoulos, G. A., & Plessa, A. (2000). Magnitude–distance relations for earthquake-induced landslides in greece. *Engineering Geology*, *58*(3-4), 377–386.

Peng, Z., Ben-Zion, Y., Michael, A. J., & Zhu, L. (2003). Quantitative analysis of seismic fault zone waves in the rupture zone of the 1992 landers, california, earthquake: evidence for a shallow trapping structure. *Geophysical Journal International*, *155*(3), 1021–1041.

Perrin, C., Manighetti, I., Ampuero, J.-P., Cappa, F., & Gaudemer, Y. (2016). Location of largest earthquake slip and fast rupture controlled by along-strike change in fault structural maturity due to fault growth. *Journal of Geophysical*

Research: Solid Earth, *121*(5), 3666–3685.

Refice, A., & Capolongo, D. (2002). Probabilistic modeling of uncertainties in earthquake-induced landslide hazard assessment. *Computers & Geosciences*, *28*(6), 735–749.

Roback, K., Clark, M. K., West, A. J., Zekkos, D., Li, G., Gallen, S. F., … Godt, J. W. (2018). The size, distribution, and mobility of landslides caused by the 2015 mw7. 8 gorkha earthquake, nepal. *Geomorphology*, *301*, 121–138.

Saygılı, G., & Rathje, E. M. (2008). Empirical predictive models for earthquake-induced sliding displacements of slopes. *Journal of Geotechnical and Geoenvironmental Engineering*, *134*(6), 790–803.

Song, S. G., Beroza, G. C., & Segall, P. (2008). A unified source model for the 1906 san francisco earthquake. *Bulletin of the Seismological Society of America*, *98*(2), 823–831.

Spudich, P., & Olsen, K. (2001). Fault zone amplified waves as a possible seismic hazard along the calaveras fault in central california. *Geophysical Research Letters*, *28*(13), 2533–2536.

Tromp, J., Komatitsch, D., & Liu, Q. (2008). Spectral-element and adjoint methods in seismology. *Communications in Computational Physics*, *3*(1), 1–32.

Weng, H., & Ampuero, J.-P. (2019). The dynamics of elongated earthquake ruptures. *Journal of Geophysical Research: Solid Earth*.

Xu, C., Xu, X., Tian, Y., Shen, L., Yao, Q., Huang, X., … Ma, S. (2016). Two comparable earthquakes produced greatly different coseismic landslides: The 2015 gorkha, nepal and 2008 wenchuan, china events. *Journal of Earth Science*, *27*(6), 1008–1015.

Yalçıner, A. C., Altinok, Y., Synolakis, C. E., Borrero, J., Imamura, F., Ersoy, S., … others (2000). Tsunami waves in izmit bay. *Earthquake Spectra*, *16*(SUPPL. A), 55–62.